Modeling the effect of prior austenite grain size on bainite formation kinetics

Avila, Daniel dos Santos; Offerman, S. Erik; Santofimia, Maria J.

DOI
10.1016/j.actamat.2024.119656

Publication date
2024

Document Version
Final published version

Published in
Acta Materialia

Acta Materialia 266 (2024) 119656

Contents lists available at ScienceDirect

Acta Materialia

journal homepage: www.elsevier.com/locate/actamat

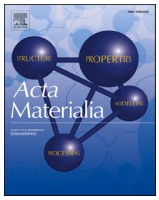

Modeling the effect of prior austenite grain size on bainite formation kinetics

Daniel dos Santos Avila *, S. Erik Offerman, Maria J. Santofimia

Department of Materials Science and Engineering, Delft University of Technology, Mekelweg 2,2628 CD, Delft, The Netherlands

ARTICLE INFO

Keywords:
Bainite
grain size
theory and modeling
phase transformation kinetics
nucleation

ABSTRACT

While experiments show that refining the prior austenite grain size can either accelerate or decelerate bainite formation in steels, kinetic models based on the successive nucleation of bainitic ferrite subunits can only predict an acceleration. In this work we develop a physically-based model for bainite kinetics assuming a displacive growth mechanism which is able to reproduce both faster and slower bainite formation kinetics induced by austenite grain refinement. A theoretical analysis of the model and comparison against published experimental data show that slower kinetics for smaller grains is favored as the difference between the activation energy for grain boundary and autocatalytic nucleation of bainite increases, and as the austenite grain refinement results in finer bainite sub-units. We also theoretically analyze the density of initially present potential nucleation sites for bainite and show that the values of density used in other published bainite nucleation models are mostly underestimated. After using physically consistent values for the density of potential nucleation sites, we were able to calculate the apparent lengthening rate of bainite sheaves which were in line with experimentally measured lengthening rates.

List of symbols

b	Burgers vector
C_1	Proportionality constant between T_h and carbon enrichment of the austenite
C_2	Proportionality constant between $T_0^{'}$ and carbon enrichment of the austenite
C_A	Number of bainite sub-units that can be formed by autocatalysis from the first bainite sub-unit nucleated at the prior austenite grain boundary
d_y	Prior austenite grain size
dN/dt	Nucleation rate of bainite
dN_A/dt	Nucleation rate of bainite by autocatalysis
dN_{GB}/dt	Nucleation rate of bainite at prior austenite grain boundaries
E_{str}	Strain energy
f	Fraction of bainite
f_A	Fraction of bainite formed by autocatalysis
f_A^{max}	Maximum fraction of bainite that can be formed by autocatalysis at time t
f_{GB}	Fraction of bainite formed by nucleation at austenite grain boundaries
f_{GB}^{max}	Maximum fraction of bainite that can be formed by nucleation at prior austenite grain boundaries
f_y	Fraction of austenite available for transformation
G_N	Universal nucleation function for bainite and Widmanstätten ferrite
G_{SB}	Stored energy of bainite
h	Planck constant
k	Boltzmann constant
K_1	Empirical constant from G_N
K_2	Empirical constant from G_N
M_s	Martensite start temperature
n	Number of atomic planes in the martensite or bainite embryo
N_m	Number of martensite plates
$N_{S,A}$	Density of potential bainite nucleation sites per bainite/austenite interface area
$N_{S,GB}$	Density of potential bainite nucleation sites per austenite grain boundary interface area
N_{tA}	Density of potential bainite nucleation sites for autocatalysis at time t
N_{tGB}	Density of potential bainite nucleation sites for grain boundary nucleation at time t

* Corresponding author.
E-mail address: D.dosSantosAvila@tudelft.nl (D.S. Avila).

https://doi.org/10.1016/j.actamat.2024.119656
Received 21 July 2023; Received in revised form 12 December 2023; Accepted 5 January 2024
Available online 6 January 2024

Q^*	Activation energy for the dissociation of dislocations during nucleation of martensite or bainite
$Q_0{}^*$	Activation energy for overcoming the short-range barriers to dislocation movement
Q_A	Activation energy for bainite nucleation by autocatalysis at time t
Q_{Ax^-}	Activation energy for bainite nucleation by autocatalysis at the nominal carbon content of the steel
Q_D	Activation energy for a carbon atom to jump from a bainite embryo to the austenite matrix
Q_{GB}	Activation energy for bainite nucleation at austenite grain boundaries at time t
Q_{GBx^-}	Activation energy for bainite nucleation by autocatalysis at the nominal carbon content of the steel
R	Universal gas constant
S_A	Area of bainite/austenite interfaces per unit volume
S_{GB}	Area of prior austenite grain boundaries per unit volume
T	Temperature
T_0	Temperature at which $\Delta G^{\gamma\to\alpha}$ is zero
$T_0^{'}$	Temperature at which $\Delta G^{\gamma\to\alpha}$ is equal to $-G_{SB}$ for the composition of austenite at time t
$T_{0\bar{x}}^{'}$	$T_0^{'}$ at the nominal carbon content of the steel
T_h	Temperature at which ΔG_m is equal to G_N for the composition of austenite at time t
$T_{h\bar{x}}$	T_h at the nominal carbon content of the steel
t	Time
u_L	Length of the bainite sub-unit
u_T	Thickness of the bainite sub-unit
u_W	Width of the bainite sub-unit
V_b	Volume of the bainite sub-unit
V_m	Volume of the martensite plate
v_L	Lengthening rate of the bainite sheaf
v^*	Activation volume for martensite or bainite nucleation
x^-	Nominal carbon content of the steel
X_b	Carbon content trapped in bainite, either in solid solution, defects, or carbides
Z	Shape factor of the austenite grain
α_m	Exponent constant of the Koistinen-Marburger equation
ΔG_m	Maximum change in Gibbs free energy for ferrite nucleation under paraequilibrium
$\Delta G^{\gamma\to\alpha}$	Difference in Gibbs free energy between austenite and ferrite with the same chemical composition
ΔQ	Difference between Q_{GB} and Q_A
δ	Effective thickness of the austenite grain boundaries
λ	Autocatalytic factor
ρ_A	Number of atoms per unit area of the closed packed plane
σ	Interfacial energy
τ_μ	Athermal resistance to dislocation movement
Ω	Atomic volume of Fe

1. Introduction

Understanding bainite formation is of great scientific and industrial interest. Bainitic steels, especially those in which cementite formation is inhibited, combine high strength with high toughness [1]. Despite having mechanical properties that are suited for several applications, such as automotive and pipelines for gas transport, their widespread use is sometimes hindered by processing difficulties such as long transformation times. Refining the prior austenite grain size has been proposed as a strategy to shorten the heat-treatments owing to faster bainite kinetics [2], but refinement of the prior austenite grain size sometimes slows down bainite formation [3]. Even though the literature has shown these opposing effects for decades, the underlying reasons behind these contradictory observations are not yet understood. It is, however, important to understand the effect of prior austenite grain size on bainite formation kinetics in order to design adequate strategies to accelerate phase transformations based on microstructure control, as well as to increase the strength and toughness of steels through microstructure refinement.

These contradictory results were already shown in early reports reflecting the effect of the prior austenite grain size on bainite formation kinetics. Davenport et al. [4] reported that the prior austenite grain size does not have any effect on the kinetics of bainite formation. Barford et al. [5], however, found that smaller grains lead to faster bainite formation, and, within the limits of their study, the reaction rate was inversely proportional to the grain size. Umemoto et al. [6] also reported faster kinetics for smaller austenite grains, and stated that the influence of the grain size on the kinetics is generally less pronounced for bainite than it is for pearlite. Graham et al. [7] and Chráska et al. [8], on the other hand, found the opposite relationship. According to their results, grain refinement led to slower bainite formation. Chráska et al. [8] suggested that the contradictory results in literature were caused by the different measuring techniques being used by different researchers.

These apparent discrepancies were clarified in a study by Matsuzaki and Bhadeshia [9], in which two steels with different chemical compositions exhibited opposite behaviors. Their work demonstrated that the contradictions were not due to differences in experimental setup, but that different steels are affected differently by changes in the prior austenite grain size. Later works, most of them using high resolution dilatometry, confirmed that both acceleration of bainite kinetics by grain refinement [2,10–12] and by grain coarsening [3,13–17] are possible.

Several mechanisms explaining the influence of the prior austenite grain size were proposed. For the acceleration of bainite kinetics by grain refinement, Barford et al. [5] argued that it occurs because bainite nucleates at the grain boundaries. For the acceleration of bainite kinetics with increasing grain size, Graham et al. [7] argued that the softer matrix of coarse-grained steels offers less resistance to the displacement caused by bainite formation.

In a unified explanation, Matsuzaki and Bhadeshia [9] linked the bainite morphology to the effect of prior austenite grain size. The researchers assumed that bainite is formed by the successive nucleation of parallel plates that organize themselves in sheaves. A sheaf is created by the nucleation of a plate of bainitic ferrite at the austenite grain boundary, and grows by the successive nucleation of new plates of bainitic ferrite. These sheaves, which contain several individual plates of bainitic ferrite, were treated as the basic unit for understanding the transformation kinetics. They hypothesized that when the growth of the bainitic sheaves is faster than their nucleation at the prior austenite grain boundary, larger prior austenite grain sizes show faster bainite formation. Inversely, when nucleation at grain boundaries is faster than the sheaf growth, a smaller grain size leads to faster kinetics. Their hypothesis was supported by metallographic evidence and a model based on the Johnson-Mehl-Avrami-Kolmogorov (JMAK) equation.

Later works that measured the kinetics of bainite formation at different prior austenite grain sizes [10–12] explained their results using the hypothesis from Matsuzaki and Bhadeshia [9]. In these works, it is argued that the observed acceleration of bainite formation by the refinement of the austenite grain size was because the reaction was nucleation-dominated. However, there is no evidence from microstructural characterization supporting these claims. It is thus not clear if Matsuzaki and Bhadeshia's hypothesis and observations can be extended to all steels.

Another challenge is incorporating the effect of the prior austenite grain size in models for bainite formation kinetics. Models such as the JMAK-type used by Matsuzaki and Bhadeshia [9] are versatile and valuable. However, since these models use many parameters with no explicit physical meaning, there is a strong limitation to how much they can be interpreted in terms of the fundamental theories and mechanisms of bainite formation. For that, a comprehensive, physically-based model for bainite formation is needed.

Ravi et al. [18] developed a model based on the diffusionless theory of bainite formation that contains only physically-based parameters and distinguishes the activation energies for grain boundary and autocatalytic nucleation. The rate of bainite formation is assumed to be controlled by the nucleation kinetics, as commonly assumed in models that adopt the diffusionless theory [1,19,20]. Another commonly shared assumption among diffusionless-theory–based models is that the density of initially present potential nucleation sites is inversely proportional to the austenite grain size [18]. This leads to the conclusion that the rate of bainite formation is also inversely proportional to the grain size – provided that all other parameters stay the same –, thus contradicting the experimental observations discussed above. Also, Ravi et al.'s [18] model does not capture the effect of prior austenite grain size on the relative contribution of autocatalysis to the overall kinetics of bainite formation, as will be shown in Section 3.1.

In this work, we modify Ravi et al.'s [18] model in order to explicitly assume that the relative contributions of grain-boundary nucleation and autocatalysis are a function of the prior austenite grain size. With the proposed modifications, the new model is able to reproduce and explain both behaviors: the acceleration and the deceleration of bainite formation by grain refinement. The model also shows good agreement with experimental data extracted from the literature. We also re-analyze and discuss important parameters of the model such as the density of potential nucleation sites and the effect of the size of the bainite sub-unit.

2. Model

There are two disputing theories for the mechanism of bainite formation. Although both theories agree that bainite is a displacive transformation that involves carbon diffusion during nucleation, they disagree on the role of carbon diffusion during growth [1,21,22]. The model used in the present work adopts the theory of diffusionless growth. According to this theory, bainite plates – also called sub-units – grow without diffusion of carbon, similarly to martensite plates, until their growth is hindered by the plastic deformation of the austenitic matrix. Such plastic deformation is induced by the stresses associated with a displacive transformation. The first sub-units are assumed to nucleate at the austenite grain boundaries, and their formation is followed by successive nucleation of new sub-units at the tips of previously formed ones – a phenomenon hereafter called autocatalysis –, thus creating the characteristic sheaf morphology. The displacive character of the transformation prevents the sheaves from growing past austenite grain boundaries.

The assumption of nucleation with carbon redistribution results in a thermodynamical requirement given by [1]:

$$\Delta G_m < G_N \tag{1}$$

The requirement from Eq. (1) states that the maximum change in Gibbs free energy for ferrite nucleation under paraequilibrium, ΔG_m, should be less than the universal nucleation function, G_N. The function G_N is an empirical function that represents the minimum driving force necessary for bainite nucleation. It is considered to be dependent only on temperature and is calculated as

$$G_N = K_1(T - 273.18) - K_2 \tag{2}$$

where K_1 and K_2 are empirical constants equal to 3.637 J mol^{-1} K^{-1} and 2540 J mol^{-1}, respectively, and T is the temperature in Kelvin [1]. The temperature in which ΔG_m and G_N are equal for a certain composition is called T_h. In addition to the nucleation, diffusionless growth also needs to be possible for bainite formation, which gives rise to the condition expressed by Eq. (3):

$$\Delta G^{\gamma\to\alpha} < -G_{SB} \tag{3}$$

in which $\Delta G^{\gamma\to\alpha}$ is the difference in Gibbs free energy between austenite and ferrite with same chemical composition, and G_{SB} is the stored energy of bainite, assumed to be 400 J mol^{-1}. The temperature in which $\Delta G^{\gamma\to\alpha}$ is equal to $-G_{SB}$ is called $T_0^{'}$. Also, the temperature in which $\Delta G^{\gamma\to\alpha}$ is zero is called T_0 [1]. According to this theory, bainite nucleation and growth can only happen in temperatures below both $T_0^{'}$ and T_h.

2.1. Overview of Ravi's model

The model developed by Ravi et al. [18] is based on the kinetics of bainite nucleation, which is split into two components: grain boundary nucleation and autocatalysis. Grain boundary nucleation is the one that takes place at the prior austenite grain boundaries (γ/γ interface). Autocatalysis, or autocatalytic nucleation, is the one that takes place at the interface between the bainitic ferrite and the austenite (α_b/γ interface). In this manuscript, a brief overview of this model is provided for better understanding of the contributions proposed.

The overall bainite nucleation rate, dN/dt, is given by the sum of the nucleation rates of these two components, respectively dN_{GB}/dt and dN_A/dt, according to Eq. (4).

$$\frac{dN}{dt} = \frac{dN_{GB}}{dt} + \frac{dN_A}{dt} \tag{4}$$

The nucleation rate at the prior austenite grain boundaries is calculated using Eq. (5)

$$\frac{dN_{GB}}{dt} = \frac{kT}{h} N_{tGB} \exp\left(-\frac{Q_{GB}}{RT}\right) \tag{5}$$

where k is Boltzmann's constant, T is the temperature in Kelvin, h is Planck's constant, N_{tGB} is the density of potential nucleation sites for nucleation at prior austenite grain boundaries at time t, Q_{GB} is the activation energy for nucleation at prior austenite grain boundaries, and R is the universal gas constant. The density of potential nucleation sites was derived by van Bohemen et al. [20] based on Magee's analysis of the nucleation of martensite [23], and is calculated as

$$N_{tGB} = \frac{6\delta}{d_\gamma}\frac{\alpha_m}{V_b}(T_h - T)f_\gamma \tag{6}$$

where δ is the effective grain size thickness, taken as 1 nm, α_m is the exponent from the Koistinen-Marburger equation for the given chemical composition, d_γ is the prior austenite grain size, V_b is the volume of the bainite sub-unit, and f_γ is the fraction of austenite available for transformation.

Similarly, the nucleation rate for autocatalysis is calculated applying:

$$\frac{dN_A}{dt} = \frac{kT}{h} N_{tA} \exp\left(-\frac{Q_A}{RT}\right) \tag{7}$$

where

$$N_{tA} = \frac{6\delta}{d_\gamma}\frac{\alpha_m}{V_b}(T_h - T)f_\gamma f \tag{8}$$

where N_{tA} is the density of potential nucleation sites for autocatalytic bainite formation at time t, Q_A is the activation energy for autocatalytic nucleation of bainite, and f is the total fraction of bainite.

Immediately after its nucleation and diffusionless growth, a bainite sub-unit is supersaturated in carbon. The excess carbon can induce the precipitation of carbides and/or partition to the austenite. As the carbon content of austenite increases as a result of said partitioning, the composition-dependent limiting temperatures for bainite formation, T_h and T_0', decrease, and are calculated as

$$T_h = T_{h\bar{X}} - C_1 f\left(\frac{\bar{X} - X_b}{1 - f}\right) \tag{9}$$

$$T_0^{'} = T_{0\bar{X}}^{'} - C_2 f\left(\frac{\bar{X} - X_b}{1 - f}\right) \tag{10}$$

where $T_{h\overline{X}}$ and $T_{0\overline{X}}^{'}$ are respectively T_h and T_0' for the nominal carbon content, C_1 and C_2 are proportionality constants, $\overline{X}$ is the nominal carbon atomic fraction, and X_b is the atomic fraction of carbon that stays in the bainite, whether in solid solution or in the form of carbides.

A lower T_h implies a smaller undercooling for bainite nucleation, which results in a higher activation energy. The activation energies are then calculated as

$$Q_{GB} = Q_{GB\overline{X}} + K_\Gamma C_1 f\left(\frac{\overline{X} - X_b}{1-f}\right) \tag{11}$$

$$Q_A = Q_{A\overline{X}} + K_\Gamma C_1 f\left(\frac{\overline{X} - X_b}{1-f}\right) \tag{12}$$

where $Q_{GB\overline{X}}$ and $Q_{A\overline{X}}$ are the respectively initial activation energies for grain boundary and autocatalytic nucleation when the carbon content in the austenite is the nominal carbon content of the steel, Q_{GB} and Q_A are respectively the instantaneous activation energy for grain boundary and autocatalytic nucleation, considering carbon enrichment of the austenite, and K_Γ is a proportionality constant [24].

The fraction of available austenite decreases both because it decomposes during bainite formation, and because carbon enrichment will decrease T_0', thus hindering the activation of some potential nucleation sites. At any given time, the fraction of austenite available for transformation is the given by

$$f_\gamma = (1-f)\left(\frac{T_0^{'} - T}{T_{0\overline{X}}^{'} - T}\right) \tag{13}$$

Finally, the nucleation rate is multiplied by the volume of the bainite sub-unit in order to calculate the rate of bainite formation, df/dt:

$$\frac{df}{dt} = \frac{dN}{dt} V_b \tag{14}$$

2.2. Proposed modification of Ravi's model

In the model developed by Ravi et al., the fraction of bainite nucleated at grain boundaries and by autocatalysis are distinguished. At any given stage of the transformation, the relative contribution of the two nucleation sites to the overall rate of bainite formation is determined solely by the difference in their activation energies. However, it is reasonable to expect that microstructural features, such as the prior austenite grain size and the size of the bainite sub-unit, would also influence the relative contribution of grain boundary nucleation and autocatalysis to the overall kinetics. Also, the austenite grain size and the size of the bainite sub-unit should limit the total fraction of bainite that can nucleate at each site. In order to tackle both aspects, the geometrical assumption illustrated in Fig. 1 is proposed.

Fig. 1a shows that at the start of bainite formation only grain boundary nucleation sites are present. The maximum fraction of bainite that can be formed from these nucleation sites, f_{GB}^{max}, depends on the prior austenite grain size, d_γ, and on the length of the bainite sub-unit, u_L. This maximum fraction is given by Eq. (15):

$$f_{GB}^{max} = Z\frac{u_L}{d_\gamma} \tag{15}$$

where Z is a shape factor equal to 3.35 for a tetrakaidecahedron-shaped austenite grain [25].

Similar to f_{GB}^{max}, the maximum fraction of bainite that can be formed by autocatalysis, f_A^{max}, can be defined. However, unlike f_{GB}^{max}, f_A^{max} varies during the transformation. At the beginning of the transformation, when no bainite is formed, it is not possible to have autocatalysis. Fig. 1b shows that after the first sub-unit of bainite is formed at the austenite grain boundary, new nucleation sites are created at the bainitic-ferrite/austenite interface, and autocatalysis can start. Considering that the first bainite sub-unit nucleated at the grain boundary can give rise to C_A bainite sub-units by autocatalysis, the change in f_A^{max} promoted by a change in the fraction of bainite nucleated at the grain boundaries, f_{GB}, can be calculated by Eq. (16)

$$df_A^{max} = C_A\left(1 - f_A^{max}\right)df_{GB} \tag{16}$$

where df_A^{max} is an infinitesimal change to f_A^{max} induced by df_{GB}, an infinitesimal change to f_{GB}. The term $(1 - f_A^{max})$ is inserted to account for hard impingement. Integrating both sides of Eq. (16) with the boundary conditions of $f_A^{max} = 0$ for $f_{GB} = 0$, and $f_A^{max} = 1 - f_{GB}^{max}$ for $f_{GB} = f_{GB}^{max}$ (Fig. 1c), results in Eq. (17) and (18):

$$C_A = \frac{\ln\left(f_{GB}^{max}\right)}{f_{GB}^{max}} \tag{17}$$

$$f_A^{max} = 1 - \exp\left(\frac{f_{GB}}{f_{GB}^{max}}\ln f_{GB}^{max}\right) \tag{18}$$

The boundary condition of $f_A^{max} = 1 - f_{GB}^{max}$ when $f_{GB} = f_{GB}^{max}$ is not necessarily true. Sheaves of bainite may grow until they are halted by the austenite grain boundaries, such that the sheaves containing the plates marked as f_A in Fig. 1c actually occupy some of the area initially marked as f_{GB}^{max}. The proposed boundary condition is then a simplification of a more complex problem, and it was chosen so that $f_{GB}^{max} + f_A^{max}$ tends towards unity as the reaction progresses.

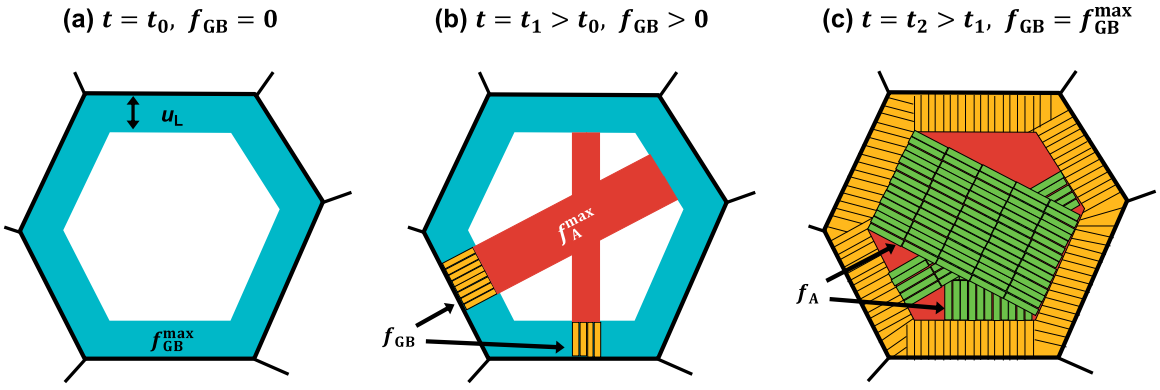

Fig. 1. Illustration representing the proposed geometrical assumption for bainite formation. A single austenite grain, at different times t, is shown. (a) The maximum fraction of bainite that can nucleate the austenite grain boundary, f_{GB}^{max}, is given by the blue-shaded area, and is defined by the length of the bainite sub-unit, u_L, and the grain size. (b) After some fraction of bainite is formed by grain boundary nucleation, marked as f_{GB}, new plates of bainite can nucleate by autocatalysis and occupy the red-shaded area indicated by f_A^{max}. (c) When $f_{GB} = f_{GB}^{max}$, all the grain interior is available for transformation, such that $f_{GB}^{max} + f_A^{max} = 1$. The green plates indicated by the arrows and marked as f_A represent the fraction of bainite nucleated by autocatalysis at time t_2.

After having defined f_{GB}^{max} and f_{A}^{max}, the two terms can be combined with Eq. (13), which includes carbon enrichment of the austenite, and used for calculating the density of potential nucleation sites at the austenite grain boundaries, N_{tGB}, and at the bainite/austenite interfaces, N_{tA}, at any given time t, as

$$N_{tGB} = N_{S,GB} S_{GB} \left(1 - \frac{f_{GB}}{f_{GB}^{max}}\right) \left(\frac{T_0^{'} - T}{T_{0\bar{X}}^{'} - T}\right) \tag{19}$$

$$N_{tA} = N_{S,A} S_{A} \left(1 - \frac{f_{A}}{f_{A}^{max}}\right) \left(\frac{T_0^{'} - T}{T_{0\bar{X}}^{'} - T}\right) \tag{20}$$

where $N_{S,GB}$ and $N_{S,A}$ are respectively the number of potential nucleation sites per unit area of austenite grain boundary and bainite/austenite interface, later discussed in Section 4.1, and S_{GB} and S_{A} are the area of the austenite grain boundaries and bainite/austenite interfaces per unit volume, respectively. The autocatalytic nucleation of bainite is commonly considered to take place at the tip of previously formed bainitic ferrite sub-units [1]. Thus, instead of considering the whole bainite/austenite interface area for calculating S_{A}, only the interface area of the tip of the sub-units is considered. The terms can then be calculated as

$$S_{GB} = \frac{Z}{d_{\gamma}} \tag{21}$$

$$S_{A} = \frac{f}{u_{L}} \tag{22}$$

While the concentrations of potential nucleation sites, $N_{S,GB}$ and $N_{S,A}$, and the interface area of prior austenite grain boundaries, S_{GB}, are constant, the interface area of the sub-units tip, S_{A}, depends on the fraction of bainite existing at given time.

In order to calculate the rate of bainite nucleation, Eqs. (19) and (20) are used in Eqs. (5) and (7), changing the way in which Ravi et al. calculated the number density of potential nucleation sites.

By comparing Eqs. (19) and (20) with Eqs. (6), (8), and (13) it can be seen that in the proposed model the saturation of nucleation sites for grain boundary nucleation and autocatalysis are distinguished through the terms $1 - f_{GB}/f_{GB}^{max}$ and $1 - f_{A}/f_{A}^{max}$. In Ravi's model, site saturation is treated as if it were equal for both grain boundary and autocatalysis, through the use of the single term $1 - f$.

2.3. Input parameters

Most of the input parameters needed for the model can be measured, calculated from empirical equations, or extracted from thermodynamic databases as described by Ravi et al. [18]. However, because of the modifications proposed here, four new input parameters are needed: $N_{S,GB}$, $N_{S,A}$, V_{b}, and u_{L}. Note that although V_{b} appears in the equations from Ravi et al. [18], it gets canceled out eventually (see Eqs. (5)–(8) and (14)). For the purpose of the present work, both $N_{S,GB}$ and $N_{S,A}$ were taken as 10^{16} m^{-2}, following van Bohemen [26]. V_{b} is calculated as $u_{T} \cdot u_{W} \cdot u_{L}$, where u_{T} and u_{W} are the thickness and the width of the bainite sub-unit. In the present work, the sub-unit was considered to be a plate with $u_{W} = u_{L} = 6 \cdot u_{T}$, following Azuma et al. [27]. The values chosen for those parameters are discussed in Section 4.1. The fraction of carbon trapped in the bainite, X_{b}, and the activation energies, Q_{GB} and Q_{A}, are fitting parameters, as in Ravi et al.'s model.

3. Results

This section starts with a theoretical analysis of the model, focusing on the predicted influence of the prior austenite grain size on the bainite formation, and the differences with respect to the results obtained following the model developed by Ravi et al. [18]. Then, the model is validated by comparison against the experimental data.

3.1. Theoretical analysis of the model

The model was first theoretically analyzed by simulating kinetic curves of bainite formation using hypothetical input parameter values that result in realistic transformation rates. Then, the effect of prior austenite grain size was also theoretically studied for different model input parameter values. All the parameters used in the simulations of this section are given in the graphs and captions of Fig. 2 and Fig. 3.

Fig. 2 shows the simulated kinetics of bainite formation during isothermal holding. The simulated curve follows a sigmoidal-like shape, resembling the experimentally measured curves of bainite formation. Because the model distinguishes the fraction of bainite per nucleation site, the curves for bainite nucleated at the austenite grain boundaries and by autocatalysis can be calculated individually, as shown in Fig. 2a. The curve for f_{GB} follows a logarithmic shape approaching a limiting value. For the case presented in Fig. 2, since there is no carbon enrichment of the austenite ($X_{b} = \bar{X}$), the limiting value for f_{GB} is given by f_{GB}^{max}. The f_{A} curve, on the other hand, follows a sigmoidal-like shape. For the present case, in which there is no carbon enrichment, f_{A} approaches $1 - f_{GB}^{max}$, so that the total fraction of bainite, f, tends towards unity.

Fig. 2b shows the rate of bainite formation distinguished by nucleation site. At the beginning of the transformation, the rate of bainite formation comes from grain boundary nucleation only. As the reaction progresses, potential nucleation sites are created at the bainite/austenite interface, and autocatalysis starts contributing to the total rate of bainite formation.

Many of the models that adopt the diffusionless theory of bainite formation use a so-called autocatalytic factor [18–20]. The autocatalytic factor, λ, is used to relate the rate of bainite nucleation at the grain boundaries, $\dot{N}_{GB}$, to the nucleation rate by autocatalysis, $\dot{N}_{A}$, through the general expression $\dot{N}_{A} = \lambda f \dot{N}_{GB}$. In the present model, no autocatalytic factor was used. However, by isolating λ in the general formula present in other models, an autocatalytic factor can be derived and calculated using the outcome of the present model according to Eq. (23).

$$\lambda = \frac{1}{f} \frac{\dot{N}_{A}}{\dot{N}_{GB}} \tag{23}$$

The calculated autocatalytic factor is shown in Fig. 2c. Unlike in other bainite models, where it is usually taken as a value to be fitted, in the present model the autocatalytic factor is an outcome. The autocatalytic factor depends on the interplay between parameters such as the prior austenite grain size, size of the bainite sub-unit, and the difference between the activation energies Q_{GB} and Q_{A}, which in turn depends on the chemical composition, temperature, and dislocations created during bainite formation. Also, the factor is not constant, but varies throughout the whole transformation.

The predicted effect of the prior austenite grain size on the bainite formation kinetics is presented in Fig. 3. Depending on the difference between the activation energies for grain boundary and autocatalytic nucleation, $\Delta Q = Q_{GB} - Q_{A}$, and on the variation of the thickness of the bainite sub-unit as a function of the prior austenite grain size, different behaviors are observed.

When the activation energies Q_{GB} and Q_{A} were considered to differ by only 5 kJ mol^{-1}, a smaller grain size led to faster bainite formation. But when Q_{A} was smaller than Q_{GB} by 15 kJ mol^{-1}, a larger prior austenite grain size led to a faster bainite formation (see Fig. 3a). This indicates that as the difference ΔQ between activation energies increases, the kinetics of bainite formation by autocatalysis tends to overcome the kinetics of bainite formation at austenite grain boundaries, ultimately leading to the observation of a faster bainite formation for larger prior austenite grain sizes.

In Fig. 3a, u_{T} was considered to be independent of the prior austenite

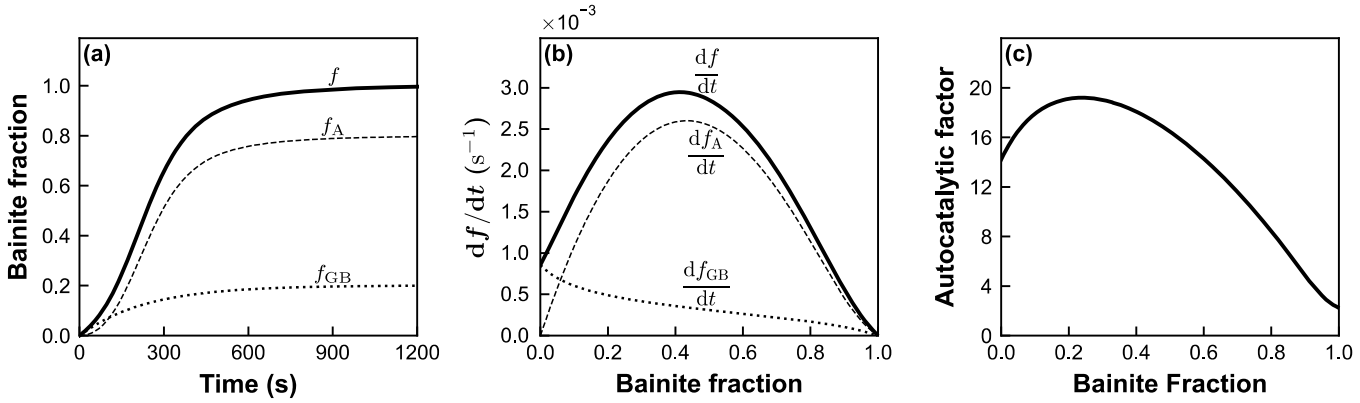

Fig. 2. Simulated kinetics of bainite formation considering the parameters: $T = 300$ °C, $d_\gamma = 10$ μm, $Q_{GBx^-} = 200$ kJ mol^{-1}, $Q_{Ax^-} = 195$ kJ mol^{-1}, $u_T = 0.100$ μm, and $X_b = X^-$. (a) Fraction of bainite over time, distinguishing the total fraction, f, the fraction nucleated by autocatalysis, f_A, and the fraction nucleated at austenite grain boundaries, f_{GB}. (b) Rate of bainite formation, also showing the total rate and distinguishing individual components by nucleation site. (c) Autocatalytic factor calculated by Eq. (23).

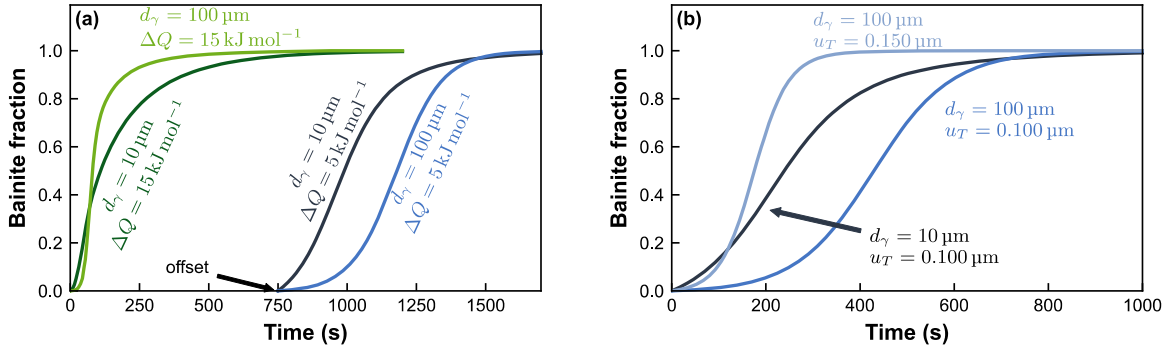

Fig. 3. Simulated curves showing the predicted effect of varying the prior austenite grain size from 10 to 100 μm on the bainite formation kinetics. The fixed parameters used were $T = 300$ °C, $Q_{GBx^-} = 200$ kJ mol^{-1}, and $X_b = X^-$, while ΔQ ($Q_{GB} - Q_A$) or u_T were varied. (a) On the left, simulated curves for $\Delta Q = 15$ kJ mol^{-1}. On the right and offset by 750 s, simulated curve for $\Delta Q = 5$ kJ mol^{-1}. In all cases, u_T was taken as 0.100 μm. (b) Curves for $\Delta Q = 5$ kJ mol^{-1}. For $d_\gamma = 10$ μm, $u_T = 0.100$ μm. For $d_\gamma = 100$ μm, two curves are shown: one considering the thickness of the sub-unit does not change by varying the grain size, and one considering that because of the increase in grain size the thickness of the sub-unit increases to 0.150 μm.

grain size. But in reality u_T might be different for different austenite grain sizes. In the present model, the nucleation rate is multiplied by the volume of the sub-unit to yield the rate of bainite formation, and thus a larger sub-unit speeds up the transformation. This possibility was explored in the simulation shown in Fig. 3b.

In Fig. 3b, the two curves from Fig. 3a corresponding to $\Delta Q = 5$ KJ mol^{-1}, for which smaller austenite grains led to a faster transformation, are shown again and complemented by a third simulated curve. In the latter, it is considered that by increasing the prior austenite grain size from 10 to 100 μm the thickness of the sub-unit increases from 0.100 to 0.150 μm. As a result, the effect of the grain size was reversed, and a larger prior austenite grain size resulted in a faster overall bainite formation.

The theoretical analysis described in this section indicates that the proposed model is capable of reproducing both the acceleration as well as the deceleration of bainite formation by the refinement of the prior austenite grain size. To our knowledge, and based on our analysis of other published models of bainite formation [18,20,27–29], the model proposed here is the only one that is able to simulate these two possible effects.

None of the results shown in this section considered the carbon enrichment of the austenite. However, we have repeated the simulations considering the carbon enrichment of austenite by choosing different values for X_b (section S1 and Fig. S1 to S3 in the supplementary materials) and we did not find any influence of the carbon enrichment of the austenite on the effect of the prior austenite grain size on bainite formation kinetics.

3.2. Comparison to Ravi et al.'s model

The predicted effect of the prior austenite grain size was also analyzed for Ravi et al.'s model, and a comparison between their model and the model from the present work is shown in Fig. 4. The simulations presented in this section use parameters similar to the ones used in Section 3.1 for the proposed model, and parameters for Ravi et al.'s model that led to similar kinetics. All parameters and values are given in the graphs and caption of Fig. 4.

By comparing Fig. 4a and c with Fig. 4b and d, it is evident that the model from Ravi et al. predicts a much greater influence of the prior austenite grain size on the kinetics of bainite formation. In the present model, the effect of grain size depends on factors such as the difference in the activation energies and the size of the bainite sub-unit. Fig. 4a and c thus represent only the specific case for the conditions used in the simulation. In Ravi et al.'s model, the rate of bainite formation is always inversely proportional to the prior austenite grain size, given that the activation energies are independent of the grain size. Hence, the trends shown in Fig. 4b and d are general for Ravi et al.'s model, and it is the only possible outcome, irrespective of the parameters used in the simulation.

As the rate of bainite nucleation at grain boundaries and by autocatalysis are distinguished in both models, it is possible to calculate the final fraction of grain boundary nucleated and autocatalytically

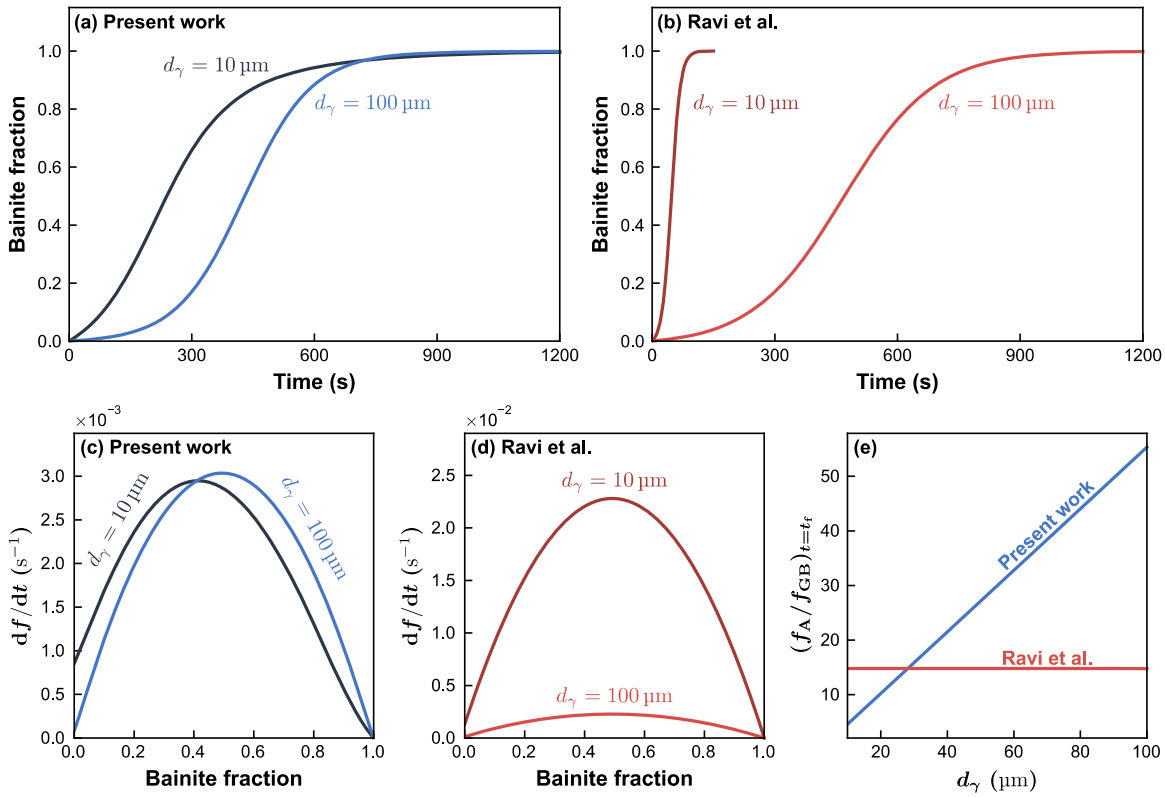

Fig. 4. Effect of the prior austenite grain size on bainite formation according to the present model and Ravi et al.'s model. In all cases $T = 300$ °C and $X_b = X^-$ were considered. For the simulations using the model from the present work, $Q_{GBx^-} = 200$ kJ mol^{-1}, $Q_{Ax^-} = 195$ kJ mol^{-1}, and $u_T = 0.100$ μm were used. In the simulations using Ravi et al.'s model, $Q_{GBx^-} = 145$ kJ mol^{-1}, $Q_{Ax^-} = 125$ kJ mol^{-1}, $T_h = 577$ °C, and $\alpha_m = 0.011$ K^{-1} were used. (a–d) Simulated bainite fraction as a function of time and the rate of bainite formation as a function of bainite fraction for both models and for $d_\gamma = 10$ μm and $d_\gamma = 100$ μm. (e) Ratio between the fraction of autocatalytic nucleated and grain boundary nucleated bainite at the end of the transformation as a function of prior austenite grain size for both models.

nucleated bainite at the end of the transformation, and then calculate their ratio. Fig. 4e shows this ratio as a function of the prior austenite grain size for both models. For the model developed in the present work, the ratio increases linearly with the prior austenite grain size, meaning that autocatalysis becomes more important for larger austenite grains. On the other hand, in the model from Ravi et al., the ratio is constant with respect to the austenite grain size.

The linear relationship observed in Fig. 4e was achieved in the present model by the introduction of the parameters f_{GB}^{max} and f_A^{max}, both a function of the prior austenite grain size and the length of the bainite sub-unit. The linearity is a direct consequence of the assumption that f_{GB} at the end of the transformation is proportional to the interface area of the prior austenite grain boundaries, S_{GB}, which in turn is inversely proportional to the prior austenite grain size, d_γ – Eq. (15) and (21). Such a relationship is derived in section S2 of the supplementary materials. The two parameters control the relative contribution of grain boundary nucleation and autocatalysis, and also limit their overall fraction. In the model from Ravi et al., on the other hand, there is no limit on the fraction of grain boundary nor autocatalytic nucleated bainite, and their relative contribution does not depend on the austenite grain size nor on the bainite sub-unit size. In Ravi et al.'s model, at any given point of the transformation, the ratio between the nucleation rates is

$$\frac{df_A/dt}{df_{GB}/dt} = f\exp\left(\frac{\Delta Q}{RT}\right) \tag{24}$$

which shows that the relative contribution of each type of nucleation site is determined solely by the difference in the activation energies, and does not include the effect of the prior austenite grain size.

3.3. Comparison against experiments

Experimental data on the kinetics of bainite formation during isothermal holding measured by dilatometry was used to validate the present model. The chemical composition, prior austenite grain size, isothermal holding temperature, thickness of the bainite sub-unit and references to the original source of the data are in Table 1, alongside the given nomenclature. The curves of bainite fraction as a function of time were used for optimizing the fitting parameters (Q_{GBx^-}, Q_{Ax^-}, and X_b), and the implementation of the differential evolution algorithm [30] in SciPy and Lmfit [31,32] was used to find the best values.

In order to investigate the effect of the transformation temperature, Steels A and B, which were treated at holding temperatures in the range of 370 to 500 °C, were first fitted to the model. Fig. 5a and b show that the present model was able to match well the experimentally observed data for both steels and at every temperature. The activation energies extracted from the fitting are shown in Fig. 5c and d and listed in Table 1, and range from 220 to 270 kJ mol^{-1}. Both Q_{GBx^-} and Q_{Ax^-} increase linearly with the temperature.

The optimal fitted values for the activation energies bear uncertainties related to the fitting procedure itself and to the uncertainty in the input parameters. The uncertainty related to the fitting procedure is relatively small and estimated as less than 0.1 kJ mol—1. The uncertainty related to the input parameters, however, is much higher. By assuming there is a 10% uncertainty in the values for the prior austenite grain size and for the sub-unit thickness, and a 50% uncertainty in the sub-unit aspect ratio, the uncertainty for Q_{GBx^-} and Q_{Ax^-} were estimated as 4% and 2%, respectively. The estimation of the uncertainty in the activation energies is detailed in section S3 of the supplementary materials.

Steels C and D were chosen for analyzing the effect of the prior

Table 1
Chemical composition, prior austenite grain size (d_γ), temperature of bainite formation (T), thickness of the bainite sub-unit (u_T), and model outputs (Q_{GBx^-}, Q_{Ax^-}, and X_b) of the steels used for the validation. The grain size of steel A is not reported in the original paper [29] and thus the value estimated by [20] is used. The thickness of the bainite sub-unit for steels A and B were not reported, and thus were calculated using the model from [33] for steel A and from [34] for steel B. Q_{GBx^-}, Q_{Ax^-} and X_b result from fitting the data to the model and assuming that Q_{GBx^-} and Q_{Ax^-} are independent of d_γ.

Steel	Ref.	Chemical composition wt.%	d_γ μm	T °C	u_T μm	Q_{GBx^-} kJ mol^{-1}	Q_{Ax^-} kJ mol^{-1}	X_b at. frac.
A	[29]	Fe–0.53C–0.69Mn–0.29Cr–0.03Al	140	500	0.327	259	261	0.0241
			140	450	0.260	244	242	0.0241
			140	425	0.227	238	232	0.0241
			140	400	0.194	224	225	0.0241
			140	375	0.160	218	217	0.0240
B	[35]	Fe–0.29C–2.39Mn–1.76Si	22	480	0.178	267	251	0.0060
			22	450	0.152	253	243	0.0077
			22	420	0.131	244	232	0.0089
			22	390	0.113	228	225	0.0086
			22	370	0.102	220	218	0.0096
C	[16]	Fe–0.25C–1.6Mn–1.25Si–1Cr–0.3Mo	16	420	0.255	259	243	0.0114
			20	420	0.296	259	243	0.0096
			76	420	0.353	259	243	0.0079
			157	420	0.416	259	243	0.0075
D	[14]	Fe–0.51C–0.83Mn–1.72Si–0.98Cr–0.25Mo–0.56Co–0.60Ni–0.04Nb	33	280	0.297	202	200	0.0068
			50	280	0.297	202	200	0.0068
			72	280	0.297	202	200	0.0068
			93	280	0.297	202	200	0.0068

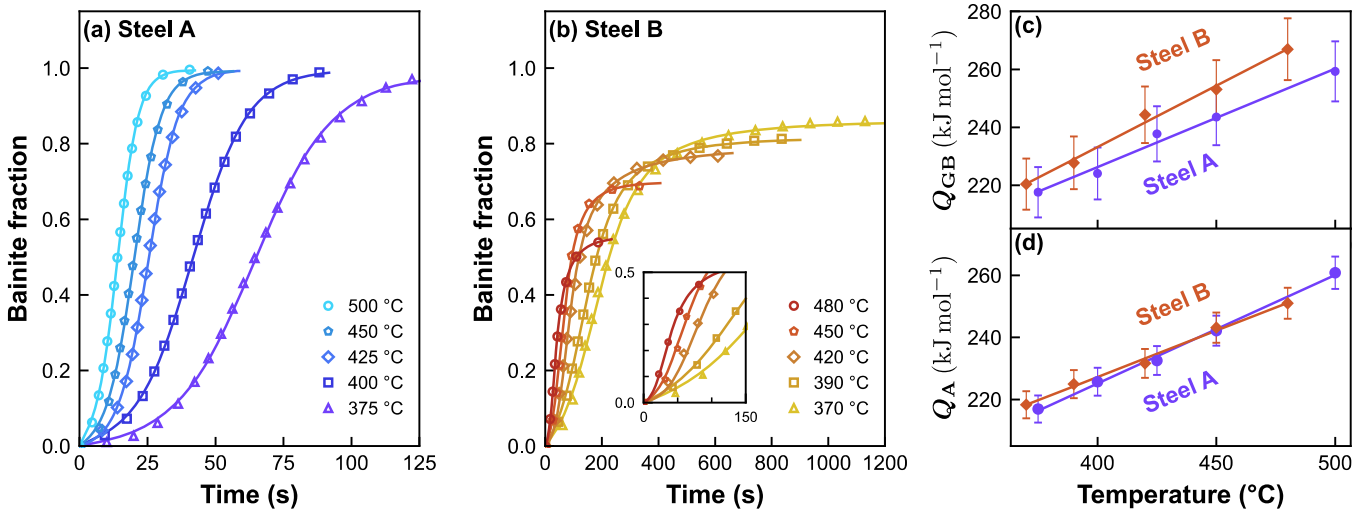

Fig. 5. Model fitted to the experimental data from steels A and B for several different holding temperatures. In (a) and (b) the markers represent the experimental data and the lines represent the fitted model. Markers in (c) and (d) show the initial activation energies extracted from the fit for Steel A (purple circle) and Steel B (red diamond), while the solid lines show linear fits. The error bars in (c) and (d) were calculated considering an uncertainty of 10% in d_γ and in u_T, and 50% in the aspect ratio of the bainite sub-unit.

austenite grain size because they show opposite behaviors. In the case of Steel C, bainite formation was accelerated by increasing the prior austenite grain size, while for Steel D the reaction was accelerated by decreasing the grain size. For each steel, samples with different grain sizes were treated isothermally at the same holding temperature.

Fig. 6 shows the experimental and modelled fraction of bainite as a function of time for the steels C and D. Because all treatments for a given steel were performed at the same holding temperature, the values of Q_{GBx^-} and Q_{Ax^-} were fitted considering that they are the same irrespective of the prior austenite grain size. The modelled curves were able to reproduce the opposing effects of the austenite grain size seen in both steels.

In the case in which bainite formation was faster for a larger prior austenite grain size (Steel C, Fig. 6a), the activation energy for grain boundary nucleation was 16 kJ mol^{-1} higher than the activation energy for autocatalytic nucleation. For Steel D (Fig. 6b), which shows the opposite effect, the difference between the activation energies was only 2 kJ mol^{-1}. This can be taken as an indication that the lengthening of bainite sheaves by the successive nucleation of bainite sub-units is relatively faster than their nucleation at grain boundaries for Steel C than it is for Steel D. This result also matches the predictions from the simulations described in Fig. 3 and the experimental observations made by Matsuzaki and Bhadeshia [9].

4. Discussion

4.1. Model parameters

4.1.1. Size of the bainite sub-unit

Both the length and the volume of the bainite sub-unit are an integral part of the present model. Their values are, however, difficult to measure. On the other hand, the thickness of the sub-units have been extensively measured and can be estimated using empirical equations available in the literature [33,34]. Then, the length can be calculated by assuming an aspect ratio – which is, however, also difficult to estimate. Based on the images from Bhadeshia et al. [37], the size of a sub-unit

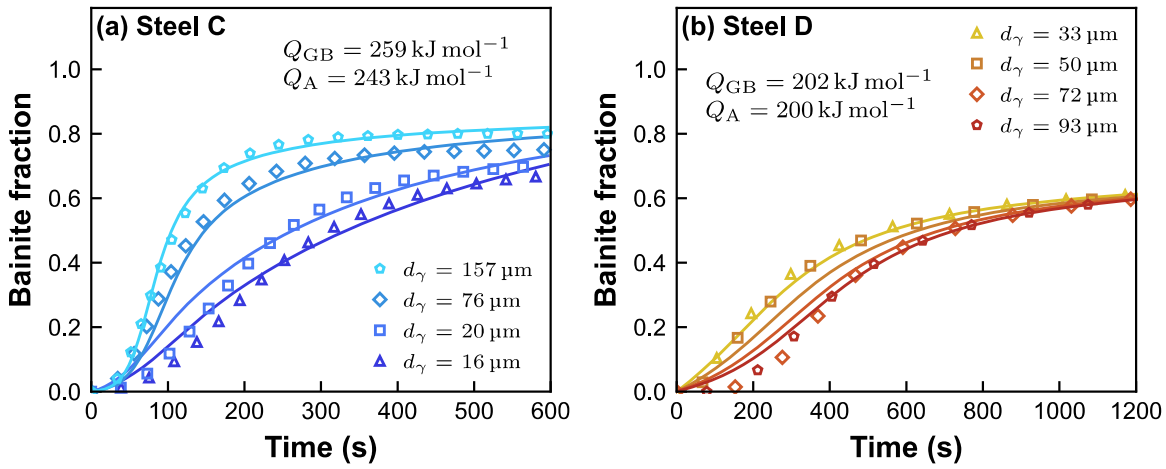

Fig. 6. Experimental data (markers) and modeled curve (solid line) of bainite formation for (a) steel C and (b) steel D at different prior austenite grain sizes, alongside the best fit values for the initial activation energies. Since the retained austenite fraction for Steel D was not reported, it was estimated using the steel models from Thermo-Calc version 2023a with the thermodynamic database TCFE12 [36].

was estimated to be 0.2 x 10 x 10 μm, which indicates an aspect ratio of 50. In-depth analysis at a higher resolution indicated that the aspect ratio could actually be in the range from 2 to 15 [38–40]. All of these values are based on a few images from transmission electron microscopy, and thus should be interpreted with care. Also, the size of the sub-unit should not be mistaken for the size of a sheaf of bainite seen by optical microscopy [41], since a sheaf is an aggregate of several individual sub-units.

Azuma et al. [27] were able to model the change from upper to lower bainite assuming an aspect ratio of 6, a value that lies in the middle of the 2 to 15 range. For that reason, the aspect ratio was assumed to be 6 in the present work. Since this estimate bears much uncertainty, and may vary depending on the chemical composition of the steel and the transformation temperature, a 50% uncertainty on the aspect ratio was considered when calculating the errors in Q_{GBx^-} and Q_{Ax^-}.

The rate of bainite formation is proportional to the volume of the bainite sub-unit in the present model. Although this differs from Ravi et al.'s model [18], in which V_b has no influence, it is in line with other models of bainite formation, such as the one from Matsuda and Bhadeshia [42]. Given that a higher V_b means that each nucleation event will give rise to a correspondingly greater fraction of bainite, it seems reasonable to assume this linear relationship.

Correctly capturing the influence of the volume of the sub-unit on the rate of bainite formation is especially important in the present work because by changing the prior austenite grain size the volume of the sub-unit may also change. And, in turn, the correlation between V_b and d_γ could define the effect of the prior austenite grain size on the kinetics of bainite formation, as shown in the simulation presented in Fig. 3b. This relation between V_b, d_γ, and the kinetics of bainite formation will be further discussed in Section 4.2.

4.1.2. Density of potential nucleation sites

According to the displacive theory of bainite formation, nucleation happens by the dissociation of dislocations, similar to martensite formation [1,43]. Because of this similarity, Magee's work on martensite nucleation [23] was used by van Bohemen [20] in order to estimate the density of initially present potential nucleation sites for bainite.

In the case of martensite, Magee assumed that there is a linear relationship between the driving force for the fcc → bcc transformation and the number of nucleation events of new martensite plates per unit volume of austenite. Following this simple assumption, Magee arrived at the same expression relating undercooling and fraction of martensite than the one found empirically by Koistinen and Marburger [44]. At small undercoolings below M_s, the number of martensite plates nucleated per unit volume of austenite is calculated as

$$N_m = \frac{\alpha_m}{V_m}(M_s - T) \tag{25}$$

where N_m is the number of martensite plates per unit volume of austenite, V_m is the average volume of martensite plates, and M_s is the martensite start temperature.

While martensite seems to nucleate in defects present inside the austenite grains, bainite seems to nucleate preferentially at the austenite grain boundaries. Thus, in order to calculate the potential nucleation sites for bainite, van Bohemen [20] scaled down Eq. (25) by the factor $6\delta/d_\gamma$ and changed the martensite-related parameters M_s and V_m by the corresponding bainite-related parameters T_h and V_b, giving rise to Eq. (6), which is also used in Ravi et al.'s model [18]. There are two factors, however, that could lead to errors in van Bohemen's [20] approach.

First, in Magee's derivation of the Koistinen-Marburger, Eq. (25), it is not the density of initially present potential nucleation sites that is calculated, but the density of plates of martensite that actually nucleate. When a potential nucleation site is activated, a plate of martensite nucleates and then grows to its final size, sweeping many other potential nucleation sites in the process. Thus, the real number of potential nucleation sites may be much higher than the number of plates that actually nucleate, and the two values should not be equated.

Also, the effect of autocatalysis has been overlooked in van Bohemen's derivation. Since Magee's equation considers the total number of martensite plates nucleated, it takes into account not only the martensite plates nucleated at pre-existing defects in austenite but the plates nucleated by autocatalysis at newly created nucleation sites (for more detail see Fig. 2 in [23]). But when adapting it to the case of bainite nucleation at defects initially present in the austenite, Eq. (25) was used as if it concerned only nucleation at pre-existing defects and did not include autocatalysis – which is not the case.

Different approaches were used in other bainite models, mostly using the density of potential nucleation sites at the austenite grain boundaries, $N_{S,GB}$, as a fitting parameter [26,27,29,42,45–49]. The values reported differ by a striking 46 orders of magnitude, varying from 10^{-30} [48] to 10^{16} per m^2 of austenite grain boundary [26]. The wide range may be partially caused by the difficulty of simultaneously fitting the activation energy and the density of potential nucleation sites.

In order to perform a quantitative analysis, the values of $N_{S,GB}$ were compared to the physically-based limits – calculated for a single austenite grain – that we propose in Fig. 7. Considering that nucleation of bainite plates at the austenite grain boundaries takes place at pre-existing defects, the number of potential nucleation sites initially

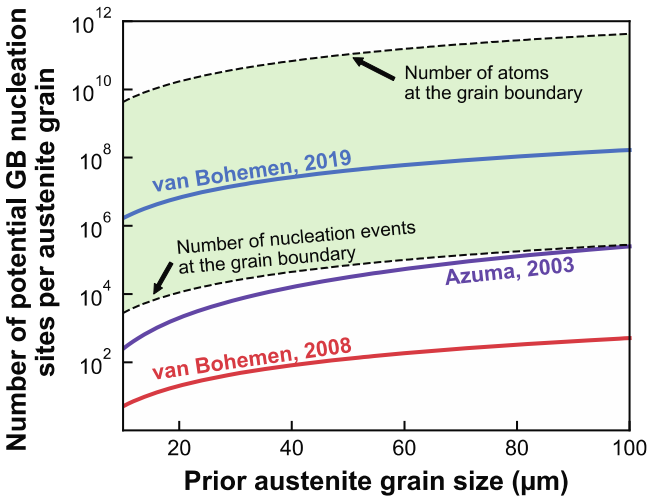

Fig. 7. Potential sites for bainite nucleation per austenite grain as a function of grain size calculated according to the models from van Bohemen, 2008 [20], Azuma [27] and van Bohemen, 2019 [26]. The calculations were performed considering $u_T = 0.100$ μm, $u_W = u_L = 0.600$ μm, $T_h - T = 100$ K, $\alpha_m = 0.011$ K^{-1}, $Z = 3.35$, and $2.5 \cdot 10^{19}$ atoms per m^2 of austenite grain boundary. The shaded area marks the region limited at the bottom by the number of nucleation events at the grain boundary necessary to occupy the whole austenite grain boundary and at the top by the number of atoms in the austenite grain boundary.

present should be *at least* as large as the number of nucleation events necessary to fully occupy the austenite grain boundary. The number of necessary nucleation events can be calculated by dividing the grain boundary area by the bainite sub-unit tip area. The *upper limit* for the potential nucleation sites is the number of atoms present at the austenite grain boundary.

Fig. 7 shows that the values reported by van Bohemen in 2019 [26], at $N_{S,GB} = 10^{16}$ m^{-2} and at the top of the observed range, are the only ones that lie inside the range given by the proposed limits. The early values found by van Bohemen in 2008 [20], Eq. (6), and used by Ravi et al. [18] and subsequent models [50,51] are three to four orders of magnitude smaller than the lower limit. The curves for most of the other cited models are not shown in Fig. 7 because they are too far from the limiting range, with most resulting in less than one potential nucleation site per austenite grain.

From the above discussion it is clear that estimating $N_{S,GB}$, either by using it as a fitting parameter or by relating it to martensite nucleation, is not straightforward. Also, the physical interpretation of the density of potential nucleation sites and the enormous discrepancy among the reported values have been overlooked in previous models of bainite nucleation. In the present work, $N_{S,GB}$ was taken as 10^{16} m^{-2}, following van Bohemen [26], because it is the only value reported so far that is within the limits shown in Fig. 7. Additionally, this value, which is equivalent to one potential nucleation site every 100 nm^2 of austenite grain boundary, is consistent with the mechanism of bainite nucleation proposed by the displacive-diffusionless theory of bainite formation [1].

Considering that bainite nucleation is similar to that of martensite, the controlling mechanism is then the dissociation of dislocations. Although the structure of grain boundaries is not always well defined, it can be sometimes well represented in terms of arrays of dislocations or similar defects [52] separated by a few atomic distances [53]. The separation of these defects is in line with the density of potential nucleation sites used in the present work. Then, a similar argument can be made for nucleation at the tip of the bainite sub-units, $N_{S,A}$, which in the present work was also taken as equal to 10^{16} m^{-2}.

The initial density of potential nucleation sites for a steel with a prior austenite grain size of 50 μm, considering $N_{S,SG}$ as 10^{16} m^{-2}, is in the order of 10^{20} to 10^{21} m^{-3}. Although it is physically consistent with the argument made in Fig. 7, it is much higher than the values reported for martensite. Based on classical small particles experiments, the density of initially-present potential nucleation sites for martensite was estimated as 10^{11} to 10^{13} m^{-3} [23].

In the case of martensite, however, 10^{11} to 10^{13} initial potential nucleation sites per m^{-3} is enough to ensure a full transformation. This is because the volume of martensite plates can be much higher than that of bainite plates, and the creation of new potential sites for nucleation by autocatalysis is much higher for martensite than for bainite. While the autocatalytic factor for bainite is usually in the order of 3 to 200 [20,28], for martensite it is reported to be in the range of 1000 [23,54,55]. Also, the fact that martensite formation is seen to start in the grain interiors and bainite formation in the grain boundaries indicates that, despite their mechanism of formation being similar, their nucleation sites are not exactly the same.

Finally, given the uncertainty in the values of $N_{S,GB}$ and $N_{S,A}$, it is important to know their effect in the model. Both values multiply the exponential term containing the activation energies for nucleation. Since the activation energies are fitted to the experimental data, any error in the density of potential nucleation sites results in an erroneous estimation of the activation energy – an overestimation of $N_{S,GB}$ leads to an overestimation of Q_{GB}, for instance. Since in all cases the same values of $N_{S,GB}$ and $N_{S,A}$ were used, any error in the assumed values resulted in roughly the same error in all values of Q_{GB} and Q_A extracted from fitting. This means that although the absolute values of Q_{GB} and Q_A reported in the present work bear this uncertainty with it, none of the trends – such as the ones in Fig. 5 and Fig. 6– are affected by this uncertainty.

4.1.3. Activation energy

The activation energies for bainite nucleation for steels A-D were found to be in the range from 200 to 270 kJ mol^{-1}. These values are higher than the ones reported in previous models, which usually range from 100 to 180 kJ mol^{-1} [18,20,42]. For steel A and B, the activation energies reported by Ravi et al. [18] were up to 120 kJ mol^{-1} lower than the ones found in the present work. This difference is due to the underestimation of the density of potential nucleation sites in previous models.

In Eq. (5) and (7), the density of potential nucleation sites multiplies the exponential term containing the activation energy for nucleation. Hence, the activation energy found by fitting the model to experimental curves of bainite formation kinetics depends on the assumed density of potential nucleation sites. In the present work, we took the number of potential nucleation sites per interface area, $N_{S,GB}$ and $N_{S,A}$, to be 10^{16} m^{-2}. Although we have explained that the assumed values are the most realistic considering the physical conditions of the transformation, here we further explore the consequences of using other values of $N_{S,GB}$ and $N_{S,A}$ in the resulting activation energies.

Fig. 8 shows the activation energy for bainite nucleation found for steel B isothermally treated at 420 °C as a function of the assumed $N_{S,GB}$ and $N_{S,A}$, which were varied from 10^6 to 10^{16} m^{-2}. Both Q_{GBx^-} and Q_{Ax^-} vary by 130 kJ mol^{-1} within this range. At 10^{10} potential nucleation sites per m^{-2}, which is the order of magnitude used by Ravi et al., Q_{GBx^-} and Q_{Ax^-} are respectively 165 and 152 kJ mol^{-1}, differing only by 3 kJ mol^{-1} from the values found by Ravi et al. (168 and 155 kJ mol^{-1}). Thus, the lower values of activation energy for bainite previously reported in other models in the literature are a consequence of such models may having underestimated the density of potential nucleation sites for bainite nucleation.

According to the displacive theory of bainite formation, there are two thermally-activated events involved in the nucleation: carbon diffusion and dissociation of dislocations [1]. The activation energy for bainite nucleation, Q, can then be understood as the sum of the individual activation energies for carbon diffusion, Q_D, and for the dissociation of dislocations, Q^* [27,56]. Rigorously, Q_D is the activation energy for a carbon atom to jump from a bainite embryo to the austenite matrix. Since this value is not known, Q_D can be approximated as the activation

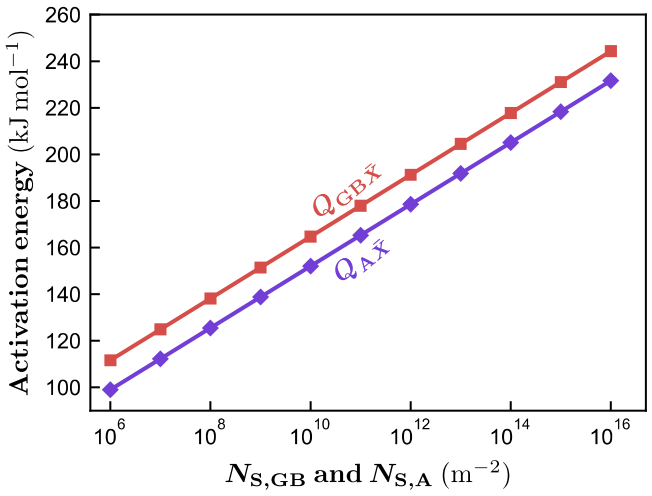

Fig. 8. Estimated activation energies for bainite nucleation in steel B isothermally treated at 420 °C as a function of the assumed values of the number of potential nucleation sites per interface area, $N_{S,GB}$ and $N_{S,A}$.

energy for carbon diffusion in the austenite, which is around 140 kJ mol^{-1} (from databases TCFE12 and MOBFE7 in Thermo-Calc). Thus, Q^* was found to vary from 60 to 130 kJ mol^{-1}, which is smaller than the activation energy for the diffusional movement of ferrite/austenite interfaces, estimated as 140 kJ mol^{-1} [57].

According to Olson and Cohen's theory of martensite nucleation [58], which has been adopted in the theory of bainite nucleation [1], Q^* can be calculated as

$$Q^* = Q_0^* + \left(\tau_\mu + \frac{\rho_A}{b}E_{str} + \frac{2\sigma}{nb}\right)v^* + \left(\frac{\rho_A}{b}v^*\right)\Delta G_m \quad (26)$$

where Q_0^* is the activation energy for overcoming the short-range barriers to dislocation movement, τ_μ is the athermal resistance to dislocation movement, ρ_A is the number of atoms per unit area of the closed packed plane, b is the Burgers vector, E_{str} is the strain energy, σ is the bainite/austenite interfacial energy, n is the number of atomic planes of the embryo, and v^* is the activation volume [1,58,59].

Since Eq. (26) has several unknown parameters (Q_0^*, τ_μ, E_{str}, σ, n, v^*), it cannot be directly used to calculate Q^*. The derivative of Eq. (26) with respect to temperature, however, can be used to estimate the activation volume for bainite nucleation. If ΔG_m is assumed to be the only temperature-dependent parameter in Eq. (26), then the derivative is calculated as

$$\frac{dQ^*}{dT} = \frac{\rho_A}{b}v^*\frac{d(\Delta G_m)}{dT} \quad (27)$$

Using the values of ΔG_m calculated in Thermo-Calc, the activation volume v^* for the grain boundary and autocatalytic nucleation of bainite in steel A is estimated as 55 and 57 Ω, respectively, and in steel B as 72 and 51 Ω, where Ω is the atomic volume of the Fe atom ($8.5 \cdot 10^{-30}$ m^3). These values are in line with the range reported by Olson and Cohen for the isothermal martensite nucleation in Fe-Ni and Fe-Ni-Mn alloys, which was from 21 to 73 Ω [58].

The slopes dQ^*/dT for steels A and B, calculated from the curves shown in Fig. 5c and d, were in the range from 272 to 386 J K^{-1}. Again, these values are close to those reported for isothermal martensite nucleation in Fe-Ni-Mn alloys, which were around 300 to 360 J K^{-1} [54,55].

4.1.4. Lengthening rate of sheaves

A sheaf of bainite is a structure formed by an aggregate of bainite sub-units that were nucleated one at the tip of the other by autocatalysis. The lengthening of bainite sheaves is not, according to the diffusionless theory, a continuous process, but rather a succession of several nucleation events. Although the present model is based on the individual nucleation events, the lengthening rate of bainite sheaves can be derived and compared with experimental values.

The apparent lengthening rate of a sheaf of bainite, v_L, can be calculated as the product of the length of a bainite sub-unit and the nucleation rate at the tip of a single sub-unit.

$$v_L = u_L\frac{kT}{h}N_{S,A}u_T u_W \exp\left(-\frac{Q_A}{RT}\right) \quad (28)$$

In Eq. (28), the product $N_{S,A} \cdot u_T \cdot u_W$ is the number of potential nucleation sites at the tip of a single bainite sub-unit.

Fig. 9 shows the lengthening rate for steel A and B calculated using the model from the present work, the model from Ravi et al., and Thermo-Calc [60]. In Ravi's model $N_{S,A}$ is not defined, and thus the number of potential nucleation sites at the tip of the individual sub-units cannot be calculated. However, for the bainitic transformation to progress, it is necessary to have at least one potential nucleation site at the tip of every sub-unit. For that reason, the term $N_{S,A} \cdot u_T \cdot u_W$ was considered to be equal to one when calculating the lengthening rate according to Ravi's model. According to the model from the present work, the number of potential nucleation sites at the tip of the bainite sub-units varied from 600 to 6000 for Steels A and B.

The lengthening rates obtained for steel A and B using the present model were in the range from 10^{-8} to 10^{-6} m s^{-1}. In comparison, using Ravi et al.'s model, lengthening rates up to 10^{-2} m s^{-1} were found, which is two orders of magnitude above the highest value reported in literature [1,60]. The unrealistically high values from Ravi et al.'s model are due to the underestimation of potential nucleation sites. Although one potential nucleation site per bainite sub-unit was assumed in the present calculation, the values of N_{tA} calculated from Eq. (8) suggest that in Ravi et al.'s model there is less than one potential nucleation site per tip of bainite sub-unit. This value is too low, since without at least one potential nucleation site per tip, the growth of a sheaf cannot progress.

For steel B, the lengthening rates calculated using the present model and using Thermo-Calc match well. For steel A, however, the rates calculated using the present model were 10 to 20 times lower. The results from Thermo-Calc simulation are closer to experimental values of steels with chemical composition similar to the one of steel B [60],

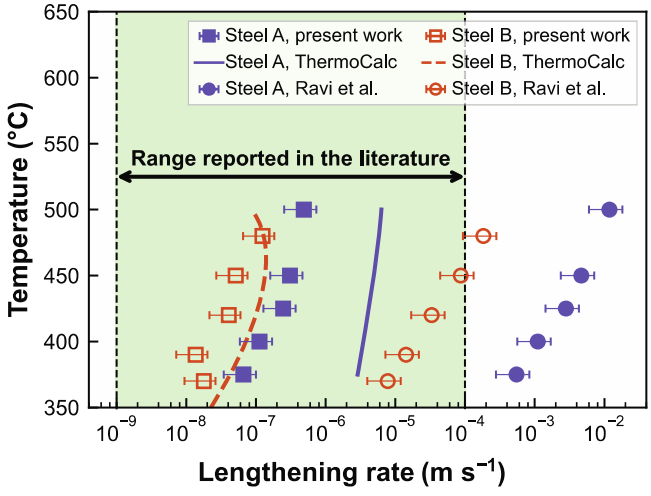

Fig. 9. Lengthening rate of bainite sheaves in steel A and B calculated according to the model from the present work, to the model from Ravi et al. [18], and to Thermo-Calc [36,60]. Shaded area represents the range of values reported in the literature so far for several steels [1,60]. The error bars were estimated considering an uncertainty of 10% in d_γ and in u_T, and 50% in the aspect ratio of the bainite sub-unit. The error associated with the Thermo-Calc could not be estimated, but based on Ref. [60] it may span more than one order of magnitude.

indicating that the present model underestimated the lengthening rate of the bainitic sheaf. However, two critical aspects need to be considered when making this comparison.

First, the model from the present work and Thermo-Calc's model use different optimization strategies. While Thermo-Calc's model used for calculating the curves in Fig. 9 was optimized to match the experimentally measured lengthening rates [60], the model from the present work was optimized to match the overall kinetics of bainite formation. Even so, the difference between Thermo-Calc's simulation and the experimentally measured lengthening rates can differ by a factor of 20 [60].

Second, the experimental data used for optimizing Thermo-Calc's model was measured either by in situ hot-stage microscopy or by measuring the longest bainite sheaf after interrupted transformation. The former technique measures the lengthening rate on the surface, which can be faster than in the bulk because of free surface effects [60]. The later technique measures the rate of the fastest growing sheaf, not the average lengthening rate.

4.2. Effect of the prior austenite grain size on bainite formation

Refining the grain size of the parent phase usually accelerates the formation of the precipitating phase. In the case of bainite, not only acceleration but deceleration have been reported. In the present work, both behaviors were successfully replicated by a single model, as shown in Fig. 3 and Fig. 6. In the model developed, the behavior that the steel will show depends on ΔQ – the difference between the activation energy for grain boundary and autocatalytic nucleation – and on how the thickness of the bainite sub-unit, u_T, varies with the prior austenite grain size.

The effect of ΔQ has been verified experimentally by Matsuzaki and Bhadeshia [9], who analyzed the microstructure after interrupted bainitic treatment of two steels showing opposite behaviors. For the steel in which bainite formation was accelerated by increasing the austenite grain size, the lengthening of sheaves was faster than their nucleation at the grain boundaries, which is consistent with a high ΔQ. Conversely, for the steel in which bainite formation was accelerated by decreasing the austenite grain size, nucleation at the grain boundaries was faster than the growth of sheaves, consistent with a small ΔQ. It is important then to discuss which aspects of the steel influence ΔQ and u_T.

From Eq. (26), the difference between Q_{GB} and Q_A can be understood in terms of different interfacial energies, σ, and different strain energies, E_{str}. While autocatalytic nucleation takes place at the α/γ interface, grain boundary nucleation takes place at a γ/γ interface, and hence they are expected to have different σ values for nucleation.

The strain energy caused by bainite formation can be decreased by self-accommodating variant pairing [61]. Hence, sub-units nucleated by autocatalysis might face a smaller strain energy barrier than the first sub-units formed at the austenite grain boundaries. This effect is of course expected to be less important at larger undercoolings, when the driving force for nucleation is much higher than the strain energy. Table 1 indeed shows that for Steel B ΔQ decreases with decreasing temperature, going from 16 kJ mol^{-1} at 480 °C to 2 kJ mol^{-1} at 370 °C. This effect is not seen in Steel A, which shows a small ΔQ of 1 kJ mol^{-1} on average throughout the whole reported temperature range.

The first bainite model to distinguish the activation energy by nucleation site is that of Ravi et al. Previous models have used instead an autocatalytic factor (λ) [20,28,48], which depends on, among other terms, ΔQ, as shows Eq. (23). A higher ΔQ translates to a higher λ. Rees and Bhadeshia [28] argued that the temporarily higher carbon concentration at the tip of bainite sub-units hinders autocatalysis, and hence proposed that the autocatalytic factor, λ, decreases linearly with the carbon content of the steel. In terms of the present model, this reasoning means a lower ΔQ as the carbon content increases.

Indeed, from analyzing the data for steel A-D, higher temperatures and lower carbon content seem to result in a higher ΔQ. The effect of carbon on ΔQ is also consistent with the work of Matsuzaki and Bhadeshia [9], in which the low carbon steel analyzed showed an acceleration of bainite formation by increasing the prior austenite grain size, and the high carbon steel showed the opposite behavior.

The reasoning above cannot explain, however, all experimental observations. There are reported cases of low carbon steel in which refining the prior austenite grain size accelerates bainite formation [10], and reported cases of high carbon steel in which refining the grain size decelerates the reaction [3,17].

Alloying elements that segregate to austenite grain boundaries may also influence ΔQ. This segregation can change the austenite grain boundary energy and locally change the driving force for bainite nucleation, thus affecting Q_{GB}. Such an effect was observed by Douguet et al [62]. by studying the addition of boron, a chemical element known for segregating to austenite grain boundaries [63]. In the boron-free version of the steel they analyzed, changing the prior austenite grain size had little impact on bainite formation kinetics. When 30 ppm of boron was added, larger prior austenite grains led to faster bainite formation kinetics, indicating that adding boron increased ΔQ.

Another aspect that defines the steel's behavior is how the size of the bainite sub-unit varies with changes in the prior austenite grain size. In martensite formation, larger austenite grains result in larger martensite plates. Consequently, increasing the prior austenite grain size accelerates the rate of isothermal martensite formation [64]. The relation between austenite grain size and size of the bainite plates, however, is not straightforward.

Since the sub-unit thickness is mainly controlled by the austenite yield strength [65], it could be expected that a smaller austenite grain size leads to finer sub-units. Note that, considering a fixed aspect ratio, a larger thickness (u_T) implies a greater volume (V_b). In van Bohemen's model for calculating the bainite plate thickness [34], the Hall-Petch effect is included when calculating the austenite yield strength, and thus the model predicts that smaller austenite grains result in finer bainite plates. This behavior has been verified experimentally for several steels, such as Steel C in the present work [16] and in the data used by van Bohemen in the model optimization.

However, the opposite effect has also been reported, in which a larger prior austenite grain size has led to the formation of finer bainite plates [66,67]. The reason for this behavior is not well explained by the currently available models, which consider u_T to be a function of austenite strength, driving force for bainite formation, and temperature. Nonetheless, it has already been shown that these three are not the only factor that define the bainite plate thickness, and that dynamic, localized factors such as the creation of dislocations at the bainite/austenite interface and the inhomogeneous distribution of carbon could play a role [65].

Although the bainite model from the present work was able to replicate the effect of the prior austenite grain size on the bainite formation kinetics, its ability to quantitatively predict the effect for a given steel composition and temperature might be limited. If an experimental curve of bainite formation at a given austenite grain size is available, the curve can be fitted to the model and the calculated ΔQ can qualitatively point to which behavior the steel might follow (see Fig. 3). For a more accurate prediction, it would be necessary to know beforehand how the size of the bainite sub-unit for the given steel changes with the prior austenite grain size – which is a short-coming of the currently available models for calculating u_T. Given the limited availability of data in the literature in which both the bainite formation curve and the size of the bainite sub-unit are reported, it was not possible to assess the predictive abilities of the model after extracting ΔQ for a given steel composition and temperature from a single curve.

The predictive abilities of the model can be improved by the atomic scale investigation of grain boundary and autocatalytic nucleation. The segregation of elements to austenite grain boundaries can influence Q_{GB} by locally changing the driving force for bainite nucleation and the boundary's interface energy. Similarly, the buildup of carbon at the tip

of bainite sub-units influences Q_A by locally decreasing the driving force for bainite nucleation. Understanding such effects can give a better insight into the factors controlling ΔQ and how it varies with temperature and chemical composition.

Another important factor that needs to be better understood is how the prior austenite grain size influences the size of the bainite sub-unit. Currently there is no single theory capable of explaining the opposing trends reported in the literature.

5. Conclusion

In the present work we developed a model that is capable of replicating both the acceleration and deceleration of the bainite formation kinetics by the refinement of the prior austenite grain size. The proposed model closely matched experimental curves of bainite formation both for steels that showed acceleration and steels that showed deceleration of bainite formation by austenite grain refinement. Two factors were found to define the effect of the prior austenite grain size on the bainite kinetics:

(i) The difference in the activation energies for grain boundary and autocatalytic nucleation, ΔQ. The larger the ΔQ, the faster the autocatalytic nucleation in comparison to grain-boundary nucleation, and the more the bainite formation tends to be accelerated by grain coarsening. Low carbon content and low undercooling seem to increase ΔQ.

(ii) The correlation between the thickness of the bainite sub-unit, u_T, and the prior austenite grain size, d_γ. If u_T increases with increasing d_γ, bainite formation tends to be faster for larger prior austenite grain sizes. The factors that define the correlation between u_T and d_γ are not yet clear.

In addition, we also analyzed the input and output parameters of bainite formation models. Most importantly, we have shown that most of the models published in the literature have underestimated the density of initially present potential nucleation sites, resulting in an underestimation of the activation energies for bainite nucleation and overestimation of the lengthening rate of bainite sheaves.

Code availability

The code necessary to reproduce the findings can be found at https://github.com/DanielDosSantosAvila/bainite-model.

Declaration of competing interest

The authors declare that they have no known competing financial interests or personal relationships that could have appeared to influence the work reported in this paper.

Acknowledgments

This project has received funding from the Research Fund for Coal and Steel under grant agreement No 899521. We would also like to acknowledge all of our partners in the RFCS-funded project MartBain, and in particular Dr. Stefan van Bohemen, Dr. Carlos Garcia-Mateo, Dr. Thomas Sourmail, and Dr. Johaness Moeller for the fruitful discussions during our meetings.

Supplementary materials

Supplementary material associated with this article can be found, in the online version, at doi:10.1016/j.actamat.2024.119656.

References

[1] H.K.D.H. Bhadeshia, Bainite in Steels Theory and Practice, 3rd ed., CRC Press, London, 2015.
[2] F.G. Caballero, H.K.D.H. Bhadeshia, Garcia-Mateo, Caballero, Bhadeshia - 2008 - Acceleration of Low-temperature Bainite, 43 (2003) 1821–1825.
[3] F. Hu, P.D. Hodgson, K.M. Wu, Acceleration of the super bainite transformation through a coarse austenite grain size, Mater. Lett. 122 (2014) 240–243, https://doi.org/10.1016/j.matlet.2014.02.051.
[4] E.S. Davenport, R.A. Grange, R.J. Hafsten, Influence of austenite grain size upon isothermal transformation behavior of SAE 4140 steel, Trans. AIME. 145 (1941) 301.
[5] J. Barford, W.S. Owen, The effect of austenite grain size and temperature on the rate of the bainite transformation, 197 (1961) 359–360.
[6] M. Umemoto, K. Horoichi, I. Tamura, Transformation kinetics of bainite during isothermal holding and continuous cooling, Tetsu-To-Hagane/J. Iron Steel Inst. Japan. 68 (1982) 461–470, https://doi.org/10.2355/tetsutohagane1955.68.3_461.
[7] L.W. Graham, H.J. Axon, The effect of austenitizing treatment on formation of lower bainite in a plain carbon steel, J. Iron Steel Inst. (1959) 361–365.
[8] P. Chráska, J. Dubský, Cyclic re-austenitizing, Mater. Sci. Eng. 41 (1979) 217–224, https://doi.org/10.1016/0025-5416(79)90141-1.
[9] A. Matsuzaki, H.K.D.H. Bhadeshia, Effect of austenite grain size and bainite morphology on overall kinetics of bainite transformation in steels, Mater. Sci. Technol. 15 (1999) 518–522, https://doi.org/10.1179/026708399101506210.
[10] L.Y. Lan, C.L. Qiu, D.W. Zhao, X.H. Gao, L.X. Du, Effect of austenite grain size on isothermal bainite transformation in low carbon microalloyed steel, Mater. Sci. Technol. 27 (2011) 1657–1663, https://doi.org/10.1179/1743284710Y.0000000026.
[11] T. Jiang, H. Liu, J. Sun, S. Guo, Y. Liu, Effect of austenite grain size on transformation of nanobainite and its mechanical properties, Mater. Sci. Eng. A. 666 (2016) 207–213, https://doi.org/10.1016/j.msea.2016.04.041.
[12] R. Ueji, Y. Kimura, K. Ushioda, T. Ohmura, T. Inoue, Bainite transformation and resultant tensile properties of 0.6%c low alloyed steels with different prior austenite grain sizes, ISIJ Int. 61 (2021) 582–590, https://doi.org/10.2355/isijinternational.ISIJINT-2020-389.
[13] G. Xu, F. Liu, L. Wang, H. Hu, A new approach to quantitative analysis of bainitic transformation in a superbainite steel, Scr. Mater. 68 (2013) 833–836, https://doi.org/10.1016/j.scriptamat.2013.01.033.
[14] Z. Li, P. Li, Y. Luo, X. Zhou, L. Qi, S. Li, Z. Wang, Effect of austenitizing temperature and prior martensite on ultra-fine bainite transformation kinetics, Metals (Basel) 9 (2019) 1–15, https://doi.org/10.3390/met9121309.
[15] S. Chen, X. Zhao, W. Xu, Effect of prior austenite grain size on bainitic transformation above and below Ms in medium Mn steel, J. Phys. Conf. Ser. (2020) 1653, https://doi.org/10.1088/1742-6596/1653/1/012043.
[16] S.M. Hasan, S. Kumar, D. Chakrabarti, S.B. Singh, Effect of prior austenite grain size on the formation of carbide-free bainite in low-alloy steel, Philos. Mag. 100 (2020) 2320–2334, https://doi.org/10.1080/14786435.2020.1764653.
[17] D. San-Martin, M. Kuntz, F.G. Caballero, C. Garcia-Mateo, A new systematic approach based on dilatometric analysis to track bainite transformation kinetics and the influence of the prior austenite grain size, Metals (Basel) 11 (2021) 324, https://doi.org/10.3390/met11020324.
[18] A.M. Ravi, J. Sietsma, M.J. Santofimia, Exploring bainite formation kinetics distinguishing grain-boundary and autocatalytic nucleation in high and low-Si steels, Acta. Mater. 105 (2016) 155–164, https://doi.org/10.1016/j.actamat.2015.11.044.
[19] M.J. Santofimia, F.G. Caballero, C. Capdevila, C. García-Mateo, C. Garcia De Andrés, Evaluation of displacive models for bainite transformation kinetics in steels, Mater. Trans. 47 (2006) 1492–1500, https://doi.org/10.2320/matertrans.47.1492.
[20] S.M.C. van Bohemen, J. Sietsma, Modeling of isothermal bainite formation based on the nucleation kinetics, Int. J. Mater. Res. 99 (2008) 739–747, https://doi.org/10.3139/146.101695.
[21] L.C.D. Fielding, The bainite controversy, Mater. Sci. Technol. (United Kingdom). 29 (2013) 383–399, https://doi.org/10.1179/1743284712Y.0000000157.
[22] S. Lin, A. Borgenstam, A. Stark, P. Hedström, Effect of Si on bainitic transformation kinetics in steels explained by carbon partitioning, carbide formation, dislocation densities, and thermodynamic conditions, Mater. Charact. (2022) 185, https://doi.org/10.1016/j.matchar.2022.111774.
[23] C.L. Magee, The nucleation of martensite. Phase Transform., ASM, 1970, pp. 115–156.
[24] S.M.C. Van Bohemen, Modeling start curves of bainite formation, Metall. Mater. Trans. A Phys. Metall. Mater. Sci. 41 (2010) 285–296, https://doi.org/10.1007/s11661-009-0106-9.
[25] J.W. Cahn, The kinetics of grain boundary nucleated reactions, Acta Metall. 4 (1956) 449–459, https://doi.org/10.1016/0001-6160(56)90041-4.
[26] S.M.C. van Bohemen, Bainite growth retardation due to mechanical stabilisation of austenite, Materialia 7 (2019) 100384, https://doi.org/10.1016/j.mtla.2019.100384.
[27] M. Azuma, N. Fujita, M. Takahashi, T. Iung, Modelling upper and lower bainite transformation in steels, Mater. Sci. Forum. 426–432 (2003) 1405–1412, https://doi.org/10.4028/www.scientific.net/MSF.426-432.1405.
[28] G.I. Rees, H.K.D.H. Bhadeshia, Bainite transformation kinetics Part 1 modified model, Mater. Sci. Technol. (United Kingdom) 8 (1992) 985–993, https://doi.org/10.1179/mst.1992.8.11.985.
[29] D. Quidort, Y.J.M. Brechet, A model of isothermal and non isothermal transformation, ISIJ Int. 42 (2002) 1010–1017.

[30] R. Storn, K. Price, Differential evolution - a simple and efficient heuristic for global optimization over continuous spaces, J. Glob. Optim. 11 (1997) 341–359, https://doi.org/10.1023/A:1008202821328.
[31] M. Newville, T. Stensitzki, D.B. Allen, M. Rawlik, A. Ingargiola, A. Nelson, LMFIT: non-linear least-square minimization and curve-fitting for Python, Astrophys. Source Code Libr. (2016), https://doi.org/10.5281/zenodo.598352.
[32] P. Virtanen, R. Gommers, T.E. Oliphant, M. Haberland, T. Reddy, D. Cournapeau, E. Burovski, P. Peterson, W. Weckesser, J. Bright, S.J. van der Walt, M. Brett, J. Wilson, K.J. Millman, N. Mayorov, A.R.J. Nelson, E. Jones, R. Kern, E. Larson, C. J. Carey, İ. Polat, Y. Feng, E.W. Moore, J. VanderPlas, D. Laxalde, J. Perktold, R. Cimrman, I. Henriksen, E.A. Quintero, C.R. Harris, A.M. Archibald, A.H. Ribeiro, F. Pedregosa, P. van Mulbregt, A. Vijaykumar, A. Pietro Bardelli, A. Rothberg, A. Hilboll, A. Kloeckner, A. Scopatz, A. Lee, A. Rokem, C.N. Woods, C. Fulton, C. Masson, C. Häggström, C. Fitzgerald, D.A. Nicholson, D.R. Hagen, D. V. Pasechnik, E. Olivetti, E. Martin, E. Wieser, F. Silva, F. Lenders, F. Wilhelm, G. Young, G.A. Price, G.L. Ingold, G.E. Allen, G.R. Lee, H. Audren, I. Probst, J. P. Dietrich, J. Silterra, J.T. Webber, J. Slavič, J. Nothman, J. Buchner, J. Kulick, J. L. Schönberger, J.V. de Miranda Cardoso, J. Reimer, J. Harrington, J.L. C. Rodríguez, J. Nunez-Iglesias, J. Kuczynski, K. Tritz, M. Thoma, M. Newville, M. Kümmerer, M. Bolingbroke, M. Tartre, M. Pak, N.J. Smith, N. Nowaczyk, N. Shebanov, O. Pavlyk, P.A. Brodtkorb, P. Lee, R.T. McGibbon, R. Feldbauer, S. Lewis, S. Tygier, S. Sievert, S. Vigna, S. Peterson, S. More, T. Pudlik, T. Oshima, T.J. Pingel, T.P. Robitaille, T. Spura, T.R. Jones, T. Cera, T. Leslie, T. Zito, T. Krauss, U. Upadhyay, Y.O. Halchenko, Y. Vázquez-Baeza, SciPy 1.0: fundamental ss for scientific computing in Python, Nat. Methods. 17 (2020) 261–272, https://doi.org/10.1038/s41592-019-0686-2.
[33] S.V. Parker, D.H.K.D.H. Bhadeshia, Modelling of Phase Transformations in Hot-Rolled Steels, Cambridge University, 1997. https://www.repository.cam.ac.uk/handle/1810/221877.
[34] S.M.C. van Bohemen, Exploring the correlation between the austenite yield strength and the bainite lath thickness, Mater. Sci. Eng. A. 731 (2018) 119–123, https://doi.org/10.1016/j.msea.2018.06.041.
[35] S.M.C. Van Bohemen, D.N. Hanlon, A physically based approach to model the incomplete bainitic transformation in high-Si steels, Int. J. Mater. Res. 103 (2012) 987–991, https://doi.org/10.3139/146.110744.
[36] J.O. Andersson, T. Helander, L. Höglund, P. Shi, B. Sundman, Thermo-Calc & DICTRA, computational tools for materials science, Calphad. Comput. Coupl. Phase Diagrams Thermochem. 26 (2002) 273–312, https://doi.org/10.1016/S0364-5916(02)00037-8.
[37] H.K.D.H. Bhadeshia, D.V. Edmonds, Mechanism of bainite formation in steels, Acta Metall. 28 (1980) 1265–1273, https://doi.org/10.1016/0001-6160(80)90082-6.
[38] I.B. Timokhina, K.D. Liss, D. Raabe, K. Rakha, H. Beladi, X.Y. Xiong, P.D. Hodgson, Growth of bainitic ferrite and carbon partitioning during the early stages of bainite transformation in a 2 mass% silicon steel studied by in situ neutron diffraction, TEM and APT, J. Appl. Crystallogr. 49 (2016) 399–414, https://doi.org/10.1107/S1600576716000418.
[39] Q. Liu, X. Zhao, X. Zhang, H. Wang, Effect of cooling temperature field on formation of shelf-like bainite in high carbon silicon steel, Mater. Sci. Eng. A. 720 (2018) 176–179, https://doi.org/10.1016/j.msea.2018.02.061.
[40] J. Nutter, J. Qi, H. Farahani, W.M. Rainforth, S. van der Zwaag, In situ TEM observations of the growth of bainitic ferrite in an Fe-0.3C-3Mn-1.5Si-0.15Mo steel, Acta Mater. 252 (2023) 118924, https://doi.org/10.1016/j.actamat.2023.118924.
[41] J. Wang, S. Van Der Zwaag, Z. Yang, H.S. Fang, Aspect ratio of bainite in steels, Mater. Lett. 45 (2000) 228–234, https://doi.org/10.1016/S0167-577X(00)00110-5.
[42] H. Matsuda, H.K.D.H. Bhadeshia, Kinetics of the bainite transformation, Proc. R. Soc. A Math. Phys. Eng. Sci. 460 (2004) 1707–1722, https://doi.org/10.1098/rspa.2003.1225.
[43] G.B. Olson, M. Cohen, A general mechanism of martensitic nucleation: part I. General concepts and the FCC → HCP transformation, Metall. Trans. A. 7 (1976) 1897–1904, https://doi.org/10.1007/BF02659822.
[44] D.P. Koistinen, R.E. Marburger, A general equation prescribing the extent of the austenite-martensite transformation in pure iron-carbon alloys and plain carbon steels, Acta Metall. 7 (1959) 59–60, https://doi.org/10.1016/0001-6160(59)90170-1.
[45] D. Gaude-Fugarolas, P.J. Jacques, A new physical model for the kinetics of the bainite transformation, ISIJ Int. 46 (2006) 712–717, https://doi.org/10.2355/isijinternational.46.712.
[46] N.V. Luzginova, L. Zhao, J. Sietsma, Bainite formation kinetics in high carbon alloyed steel, Mater. Sci. Eng. A. 481–482 (2008) 766–769, https://doi.org/10.1016/j.msea.2006.11.173.
[47] G. Sidhu, S.D. Bhole, D.L. Chen, E. Essadiqi, An improved model for bainite formation at isothermal temperatures, Scr. Mater. 64 (2011) 73–76, https://doi.org/10.1016/j.scriptamat.2010.09.009.
[48] S.B. Singh, Phase Transformations from Deformed Austenite, University of Cambridge, 1998.
[49] M.J. Santofimia, F.G. Caballero, C. Capdevila, C. García-Mateo, C.G. De Andrés, New model for the overall transformation kinetics of bainite. Part 1: the model, Mater. Trans. 47 (2006) 2465–2472, https://doi.org/10.2320/matertrans.47.2465.
[50] W. Wei, P. Retzl, E. Kozeschnik, Erwin Povoden-Karadeniz, A semi-physical α-β model on bainite transformation kinetics and carbon partitioning, Acta Mater. 207 (2021) 116701, https://doi.org/10.1016/j.actamat.2021.116701.
[51] Y. Zhang, Y. He, Y. Zhang, S. Song, F. Liu, Bainitic transformation and generalized stability, Scr. Mater. 227 (2023) 115311, https://doi.org/10.1016/j.scriptamat.2023.115311.
[52] I.S. Winter, T. Oppelstrup, T. Frolov, R.E. Rudd, Characterization and visualization of grain boundary disconnections, Acta Mater. 237 (2022) 118067, https://doi.org/10.1016/j.actamat.2022.118067.
[53] Y. Ishida, T. Hasegawa, F. Nagata, Grain-boundary fine structure in an Iron Alloy, J. Appl. Phys. 40 (1969) 2182–2186, https://doi.org/10.1063/1.1657955.
[54] G. Ghosh, V. Raghavan, The kinetics of isothermal martensitic transformation in an Fe-23.2wt.%Ni-2.8wt.%Mn alloy, Mater. Sci. Eng. 80 (1986) 65–74, https://doi.org/10.1016/0025-5416(86)90303-4.
[55] S.R. Pati, M. Cohen, Nucleation of the isothermal martensitic transformation, Acta Metall. 17 (1969) 189–199, https://doi.org/10.1016/0001-6160(69)90058-3.
[56] S.E. Offerman, N.H. Van Dijk, J. Sietsma, S. Grigull, E.M. Lauridsen, L. Margulies, H.F. Poulsen, M.T. Rekveldt, S. Van der Zwaag, Grain nucleation and growth during phase transformations, ScienceScience 298 (2002) 1003–1005, https://doi.org/10.1126/science.1076681.
[57] G.P. Krielaart, S. Van Der Zwaag, Kinetics of γ→γ phase transformation in Fe-Mn alloys containing low manganese, Mater. Sci. Technol. 14 (1998) 10–18, https://doi.org/10.1179/mst.1998.14.1.10.
[58] G.B. Olson, M. Cohen, A general mechanism of martensitic nucleation: part III. Kinetics of martensitic nucleation, Metall. Trans. A. 7 (1976) 1915–1923, https://doi.org/10.1007/BF02659824.
[59] H. Conrad, Thermally activated deformation of metals, JOM 16 (1964) 582–588, https://doi.org/10.1007/bf03378292.
[60] L. Leach, J. Ågren, L. Höglund, A. Borgenstam, Diffusion-controlled lengthening rates of bainitic ferrite a part of the steel genome, Metall. Mater. Trans. A Phys. Metall. Mater. Sci. (2019), https://doi.org/10.1007/s11661-019-05208-x.
[61] N. Takayama, G. Miyamoto, T. Furuhara, Effects of transformation temperature on variant pairing of bainitic ferrite in low carbon steel, Acta Mater. 60 (2012) 2387–2396, https://doi.org/10.1016/j.actamat.2011.12.018.
[62] P. Douguet, G. Da Rosa, P. Maugis, J. Drillet, K. Hoummada, Effect of boron segregation on bainite nucleation during isothermal transformation, Scr. Mater. 207 (2022) 114286, https://doi.org/10.1016/j.scriptamat.2021.114286.
[63] T.S. Prithiv, B. Gault, Y. Li, D. Andersen, N. Valle, S. Eswara, D. Ponge, D. Raabe, Austenite grain boundary segregation and precipitation of boron in low-C steels and their role on the heterogeneous nucleation of ferrite, Acta Mater. 252 (2023) 118947, https://doi.org/10.1016/j.actamat.2023.118947.
[64] V. Raghavan, M. Cohen, Measurement and interpretation of isothermal martensitic kinetics, Metall. Trans. 2 (1971) 2409–2418, https://doi.org/10.1007/BF02814878.
[65] A. Eres-Castellanos, J. Hidalgo, M. Zorgani, M. Jahazi, I. Toda-Caraballo, F. G. Caballero, C. Garcia-Mateo, Assessing the scale contributing factors of three carbide-free bainitic steels: a complementary theoretical and experimental approach, Mater. Des. 197 (2021) 109217, https://doi.org/10.1016/j.matdes.2020.109217.
[66] B. Chhajed, K. Mishra, K. Singh, A. Singh, Materials characterization effect of prior austenite grain size on the tensile properties and fracture toughness of nano-structured bainite, Mater. Charact. 192 (2022) 112214, https://doi.org/10.1016/j.matchar.2022.112214.
[67] K. Singh, A. Kumar, A. Singh, Effect of prior austenite grain size on the morphology of nano-bainitic steels, Metall. Mater. Trans. A. 49 (2018) 1348–1354, https://doi.org/10.1007/s11661-018-4492-8.